JOURNAL OF MATERIALS SCIENCE 31 (1996) 4467–4477

The failure of fibre composites and adhesively bonded fibre composites under high rates of test

Part III *Mixed-mode I/II and mode II loadings*

B. R. K. BLACKMAN, J. P. DEAR, A. J. KINLOCH, H. MacGILLIVRAY, Y. WANG, J. G. WILLIAMS, P. YAYLA
Department of Mechanical Engineering, Imperial College of Science, Technology and Medicine, Exhibition Road, London SW7 2BX, UK

The failure of fibre composites under high rates of test was studied in detail, using a fracture mechanics approach to determine values of the fracture energies. The present paper, Part III of the series, considers the fracture of two different fibre composite materials under mixed-mode tensile and shear (i.e. mixed-mode I/II) and shear (i.e. mode II) loadings. Part I considered the experimental aspects of the mode I fracture of the fibre composite materials, and of adhesive joints. Part II analysed the dynamic effects which are invariably associated with high-rate tests, and showed how these effects influence the observed behaviour of the test specimens.

1. Introduction

One of the most important mechanical properties of a fibre composite, consisting of continuous fibres embedded in a polymeric matrix, is its resistance to delamination. The presence of delaminations may not only lead to complete fracture, but even partial delaminations will lead to a loss of stiffness which can be a very important design consideration. A popular approach to the characterization of the propagation of interlaminar cracks has been through the application of linear elastic fracture mechanics (LEFM) which enables the critical strain-energy release rate, or fracture energy, G_c, to be deduced [1–5].

Various modes of fracture may be identified. Mode I (tensile opening) is the lowest fracture energy for isotropic materials and, thus, a crack will always propagate along a path normal to the direction of maximum principal tensile stress. Hence, a crack in an isotropic plate will propagate in mode I fracture regardless of the orientation of the initial flaw with respect to the applied stress. However, this is not necessarily the case for crack growth in fibre composites which are highly anisotropic materials. In these materials, the initial interlaminar defect is constrained and usually continues to propagate in the same plane between the laminate regardless of the orientation of the crack to the applied loads. Thus, genuine mode II (in-plane shear) global loadings are possible, although the growth of the interlaminar crack may still actually be governed by the locally induced mode I (tensile) stresses. Obviously, mixed-mode I/II failures may also be observed. Therefore, there has been considerable interest in determining values of G_{Ic}, G_{IIc} and $G_{I/IIc}$.

The present work aimed to study in detail the failure of fibre composites and adhesively bonded fibre composites under high rates of test. The present paper, Part III of the series, considers the aspects of the mixed-mode I/II and mode II fracture of the fibre composite materials. Part I [6] reported the experimental aspects of the mode I fracture of the fibre composite materials, and adhesive joints. Part II [7] analysed the dynamic effects which are invariably associated with high-rate tests, and showed that these effects may influence the observed behaviour of the test specimens.

2. Theory

2.1. Introduction

In Part I [6] of this series of papers the use of the double-cantilever beam (DCB) specimen to study mode I (tensile) failure of fibre composites and adhesively bonded joints was discussed in detail. It was shown that a problem which arises with the high-rate tests is that an accurate value of the load, P_c, cannot be measured, although the displacement, δ_c, and corresponding crack length, a, can be determined from high-speed photography; and the value of the modulus, E_{11}, used may be independently determined from three-point bend tests and ultrasonic tests. Hence, a very useful expression for the mode I interlaminar fracture energy, G_{Ic}, which does not require a direct knowledge of the load, may be derived and employed. Namely

$$G_{Ic} = \frac{3}{16}\frac{F}{N^2}\frac{\delta_c^2 h^3 E_{11}}{(a+\chi_I h)^4} \quad (1)$$

where $2h$ is the total thickness of the laminate, and the correction factors F, N and χ_I are used. The correction factors F and N account for large deflections of the

0022–2461

arm and stiffening of the arms due to the presence of the end blocks, which are used to load the specimen. The correction factor, χ_I, for mode I loading is introduced to account for end-rotation and deflection of the crack tip. The expressions and methods of obtaining values of F, N and χ_I were given previously [6].

2.2. Fixed-ratio mixed-mode (FRMM mixed-mode I/II) specimens

The fixed-ratio mixed-mode (FRMM) test arrangement containing a symmetrically inserted crack is shown in Fig. 1. In this specimen the thicknesses of the two arms are equal, i.e. $h_1 = h_2$. By analogy with Equation 1, the values of the mode I and mode II interlaminar fracture energies (i.e. G_{Ic}^m and G_{IIc}^m, respectively) which may be summed to give the mixed-mode value, $G_{I/IIc}$, are given by [3, 6, 8]

$$G_{Ic}^m = \frac{12\delta_c^2 h^3 E_{11}(a + \chi_I h)^2}{[7(a + \chi_{II}h)^3 + (L + 2\chi_I h)^3]^2} \frac{F}{N^2} \quad (2a)$$

and

$$G_{IIc}^m = \frac{9\delta_c^2 h^3 E_{11}(a + \chi_{II} h)^2}{[7(a + \chi_{II}h)^3 + (L + 2\chi_I h)^3]^2} \frac{F}{N^2} \quad (2b)$$

where [8]

$$\chi_{II} = 0.42\chi_I \quad (3)$$

and

$$G_{I/IIc} = G_{Ic}^m + G_{IIc}^m \quad (4)$$

For this specimen the ratio of mode I to mode II loading is 1.33. Hence

$$\frac{G_I^m}{G_{II}^m} = \frac{4}{3} \quad (5)$$

In the above expressions, the correction factor, χ_{II}, is that for mode II loading, and is introduced to account for end-rotation and deflection of the crack tip. The length, L, of the specimen is defined in Fig. 1. The end of the specimen is placed in a set of rollers. These prevent vertical movement of the far end of the specimen, which is held in the rollers, but allow free horizontal movement.

2.3. The end-loaded split (ELS mode II) specimen

The end-loaded split (ELS) mode II specimen test arrangement is shown in Fig. 2. By analogy with Equation 1, the value of the mode II interlaminar fracture energy, G_{IIc}, is given by [3, 6, 8]

$$G_{IIc} = \frac{9\delta_c^2 h^3 E_{11}(a + \chi_{II} h)^2}{[3(a + \chi_{II}h)^3 + (L + 2\chi_I h)^3]^2} \frac{F}{N^2} \quad (6)$$

The length, L, of the specimen is defined in Fig. 2. Also, as for the FRMM specimen, the end of the specimen is placed in a set of rollers. These prevent vertical movement of the far end of the specimen, which is held in the rollers, but which allow free horizontal movement.

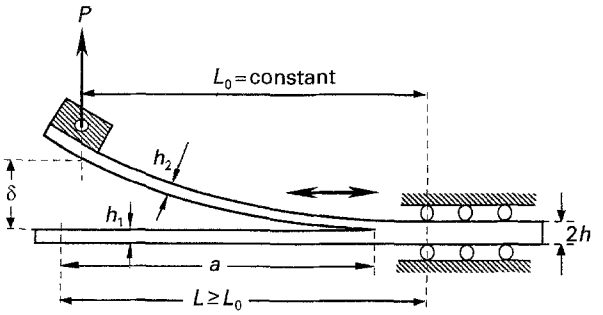

Figure 1 The fixed-ratio mixed-mode (FRMM mixed-mode I/II) composite specimen.

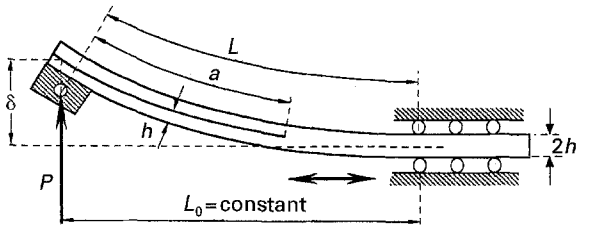

Figure 2 The end-loaded split (ELS mode II) composite specimen.

2.4. Dynamic effects

Dynamic effects may clearly be seen at the higher rates of test in the load versus time traces, as discussed above and shown later. Thus, Equations 1, 2 and 6 were employed, using measured values of displacement, crack length and modulus, in order to overcome the problems of interpreting the complex and confusing load versus time traces.

Nevertheless, as discussed in detail in Part II [7], Equations 1, 2 and 6 are still "static" analyses and do not consider dynamic effects on the measured value of G_c arising, for example, from kinetic-energy effects. In the high-rate tests, such dynamic effects on the measured G_c values must be considered. The contribution of kinetic energy to the total energy release rate has been analysed for both the mode I/II FRMM tests and the mode II ELS tests, see Appendix. (Such effects for the mode I, double-cantilever beam (DCB) test specimens are discussed in Part II [7]).

However, as discussed in the Appendix, it was found that for the present test rates, the dynamic effects on the measured value of G_c for both the mode I/II FRMM tests and the mode II ELS tests are negligible, i.e. they are always less than 3% of the measured G_c value.

3. Experimental procedure

3.1. Materials

Two different polymeric fibre composites were used in the present studies.

(i) A unidirectional carbon-fibre poly (ether–ether) ketone (PEEK) composite ("APC-2", supplied by ICI plc UK). The volume fraction of the thermoplastic PEEK matrix was nominally 35% and the carbon-fibres were "AS4" type (from Hercules Inc., USA).

(ii) A unidirectional carbon-fibre epoxy-resin composite ("Fibredux 6376C", supplied by Ciba

Composites, UK). The volume fraction of the thermosetting matrix was nominally 35% and the carbon-fibres were "T-400" type (Toray Inc., Japan).

Unidirectional laminate sheets of APC-2 were moulded using a hot press, according to the manufacturer's instructions. The epoxy/carbon-fibre composite was cured in an autoclave, according to the manufacturer's instructions.

3.2. Preparation of specimens

The fibre composite specimens were prepared in the form of the beam specimens as shown in Figs 1 and 2. For the FRMM and ELS specimens the total length of the specimens was about 200 mm. The fixed length, L_0, see Figs 1 and 2, was 100 mm. The initial delamination, a_0, was made by moulding in a double layer of aluminium foil having a total thickness of 20 μm and a length of 25 mm. This double layer insert was, however, stepped, such that the part of the insert closest to the crack tip was effectively a single layer. This resulted in a relatively low insert thickness of 12 μm which formed the initial delamination, from which crack growth occurred. Aluminium end-blocks were then bonded on to the end of the specimen where the initial delamination was present. The edge of the specimen was painted with a white typewriter correction liquid and marked at 5 mm intervals to enable the crack length to be monitored during the test.

Prior to the actual failure tests, the initial delamination in the fibre composite specimens created by the presence of the aluminium foil insert was extended to a length, a_p, of 60 mm under mode II loading i.e. the foil crack was grown by conducting a mode II test at a constant displacement rate of 0.5 mm min^{-1}. (Mode II loading was used to avoid the development of any fibre bridging which might have occurred under mode I loading.) Thus, at the onset of crack growth, the value of a_p/L_0 was 0.6. This ratio was selected because, from theoretical considerations (which included the dynamic effects arising from the high-rate tests, see Appendix), the *geometrical* criterion for stable crack growth is satisfied with a value of a_p/L_0 of 0.6 for both the FRMM and ELS test specimens.

3.3. Fracture test methods

3.3.1. Slow-rate tests

Slow-rate tests were performed using a screw-driven tensile-testing machine. The test temperature was 22 ± 1 °C. The tests were conducted in displacement control at a rate of 1 mm min^{-1}. The load and displacement were recorded using the chart recorder, and the length of the growing crack was monitored by the use of a travelling microscope mounted in front of the specimen. Each time the crack front passed a 5 mm marker on the side of the specimen, the chart was marked, so that the corresponding values of P and δ could be recorded. In the ELS and FRMM tests, the free length, L_0, was set to 100 mm. A 0.5 mm diameter pencil lead was inserted between the arms of the ELS specimens, close to the load line, to reduce friction during the mode II tests.

3.3.2. High-rate tests

Tests at intermediate rates, i.e. up to 1.67×10^{-2} m s^{-1}, were conducted using the screw-driven tensile testing machine, as described [6] previously. However, at all but the slowest rates it was, of course, not possible to monitor the crack propagation visually. Therefore, at all rates faster than 1.67×10^{-4} m s^{-1}, high-speed photography was used to record the displacement, δ, and crack length, a. At test rates in excess of 1.67×10^{-2} m s^{-1} and up to 5 m s^{-1}, a servo-hydraulic testing machine, with associated high-speed data acquisition facilities, was used. The tests were conducted at a temperature of 23 ± 2 °C.

The high-rate test rig has been described in detail previously [6]. Essentially, it consisted of a servo-hydraulic testing machine (an "Instron Model 1343"), capable of displacement rates of up to 20 m s^{-1}, and was equipped with a piezo-electric load cell with a signal amplifier. The data were acquired using a 20 MHz digital oscilloscope ("Gould 1600 series") and a "486 Personal Computer" loaded with "Dadisp" signal analysis software. Each test was photographed using a high-speed camera. This was a "Hadland 16 mm Photec (IV)" camera, with a maximum operating speed of 40 000 frames s^{-1}. The optics incorporated a 45 mm, f2.8 lens, a rotating prism and an associated half-frame image converter. A 16 mm, tungsten-balanced "7250 Eastman Film" was used to provide a high-resolution, colour record of the test. To achieve the correct exposure levels, a variable-focus tungsten spotlight was employed. This was activated immediately prior to the test to avoid any significant heating of the specimen. Incorporated into the camera was a timing-light generator which marked the film with a 1 kHz time base. To determine the actual specimen displacement, δ, and the crack length, a, at any time during the test, the film was projected, and so greatly enlarged, on to a screen; from which accurate measurements could be made. A projector was used which could project individual frames from the high-speed film.

The FRMM and ELS specimens were placed in the test rig, which was bolted on to the lower, stationary, frame of the testing machine, and the aluminium-end loading block was connected to a titanium shackle, as shown in Fig. 3. This shackle was connected, via the load cell, to a titanium "lost motion device" (LMD) which was bolted into the hydraulic ram. The purpose of the LMD device was to ensure that the ram had attained a constant velocity before motion was transferred to the specimen. The load cell was selected for its high natural frequency of 70 kHz and its short rise-time of 10 μs. Its output signal was amplified and then passed to the oscilloscope. For reference, the oscilloscope also captured the signal from the displacement transducer mounted on the ram. Thus, a record of the load versus time and the ram displacement versus time signals were captured on the oscilloscope for each test. Prior to conducting the tests, the position of the LMD was set to allow a period of pre-travel to ensure that the test was conducted at constant velocity. Tests were then performed at rates

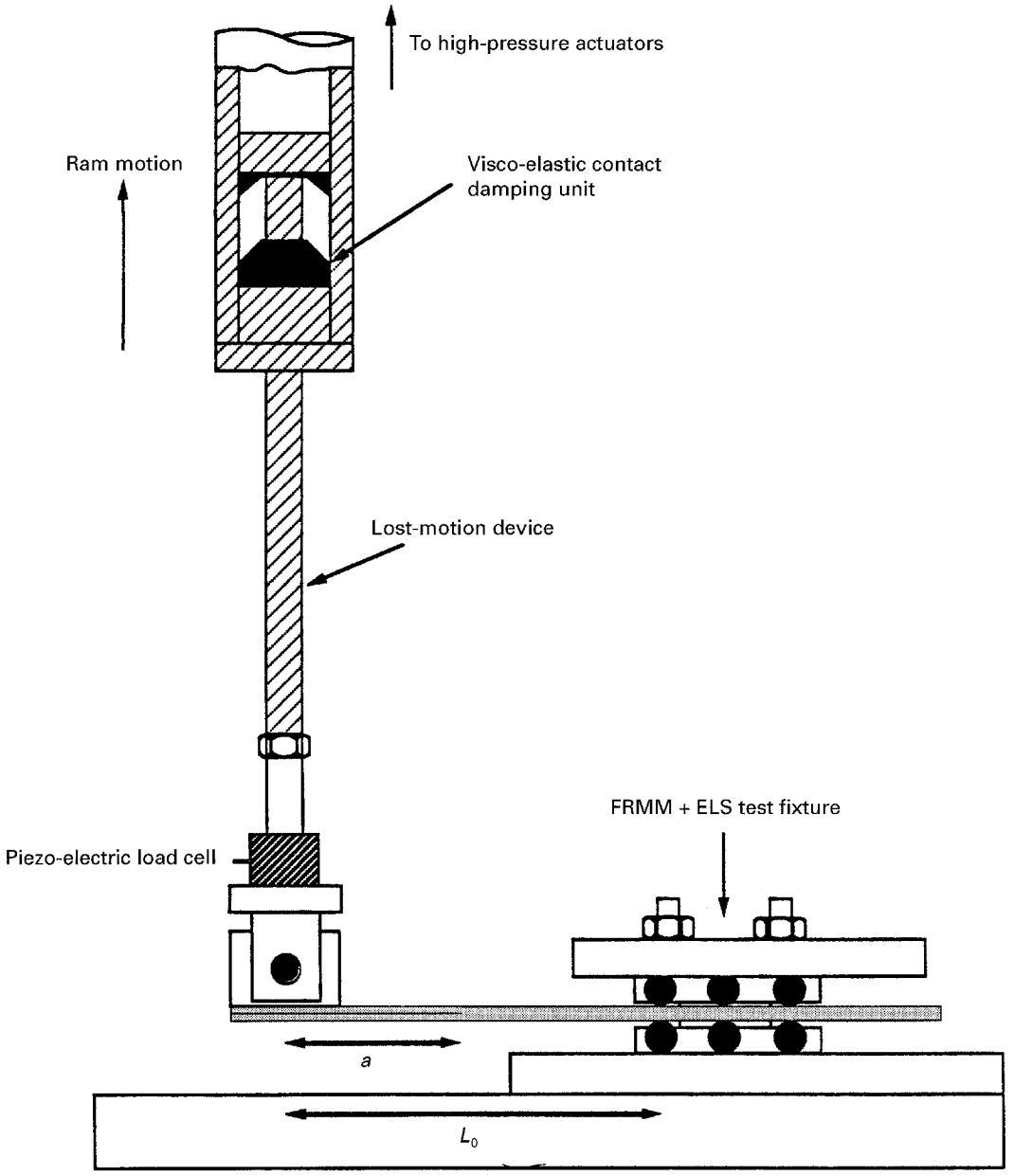

Figure 3 Schematic drawing of the high-rate test arrangement for the FRMM and ELS tests.

from 1×10^{-2} to 5 m s^{-1}. The oscilloscope and camera were triggered in order to capture the values of the load, ram displacement, specimen displacement and crack length as a function of time. Timing marks on the high-speed film record provided an accurate time base, such that the specimen displacement and crack length values could be accurately correlated to the measured values of the load. The signals were transferred to the dedicated computer, where they could be analysed using the signal analysis software.

From the above observations it is important to note that the displacement of the specimen should not be deduced from the output of the displacement transducer monitoring the position of the hydraulic ram, because this can lead to misleading results being obtained. In the present work, all displacement values used in the various equations were obtained using high-speed photography to record the actual deformations of the arms of the specimen during the test. The values of displacement so determined were not, therefore, subject to errors caused by any dynamic oscillations and/or loss of contact of the LMD during loading.

3.4. Evaluation of the axial modulus, E_{11}, of the fibre composites

3.4.1. Flexural tests

To obtain accurate values for the axial modulus of the fibre composites tested, a number of three-point bend tests were undertaken. Using composite beams, possessing an identical geometry and lay-up to those used in the fracture tests, a series of three-point bend tests were conducted at a constant displacement rate of 0.5 mm min^{-1}. In order to ensure high accuracy, an external transducer was used to measure the displacement of the beam during the test. It was noted that very good agreement was obtained between the values of the modulus calculated from beam theory following a mode I fracture test and the values measured using

the three-point bend test. The values obtained were 120 GPa for the epoxy/carbon-fibre composite and 115 GPa for the PEEK/carbon-fibre composite.

3.4.2. Ultrasonic measurements

The moduli of the fibre composites were also measured using an ultrasonic technique. Ultrasonic tests were conducted in order to investigate whether the moduli of any of the fibre composites were significantly dependent upon the strain rate. Clearly, when undertaking fracture tests at rates of up to 5 m s^{-1}, it is important to use the correct values of E_{11} in the beam-theory equations when calculating values of G_c. The details of the method have been reported previously [6]. It is sufficient to note that the values were found to be independent of the frequency used, and were in excellent agreement with the values obtained from the three-point bend tests, which were conducted at relatively slow rates of test. Thus, the static low-rate values of E_{11} for the epoxy and PEEK composites were used in Equations 2 and 6.

4. Results and discussion

4.1. Fixed-ratio mixed-mode (FRMM mode I/II) specimens

For the fixed-ratio mixed-mode (FRMM) tests the values of G_{Ic}^m, G_{IIc}^m and $G_{I/IIc}$ were obtained using Equations 2a and b and 4. For these tests, the ratio of mode I to mode II loading is 4:3, see Section 2.2.

For the PEEK/unidirectional carbon-fibre composite, the crack propagation was unstable at all rates except for the very slowest rates employed; i.e. unstable crack propagation was always observed above a test rate of 3.3×10^{-5} m s^{-1}. The instability was such that no arrest point was observed until the crack reached the roller-rig, when $a = L$. Hence, the values of G_{Ic}^m and G_{IIc}^m shown in Fig. 4 are for the onset of crack growth. As may be seen, there is no dramatic effect of rate upon the values of these parameters, although there is a tendency for the values of G_{Ic}^m and G_{IIc}^m to decrease somewhat at the highest rates of displacement.

A similar picture emerges for the epoxy/unidirectional carbon-fibre composite, except for this material, crack propagation was stable up to a somewhat higher rate of test of 1×10^{-2} m s^{-1}, after which unstable crack propagation again resulted. The values of the interlaminar fracture energies for the onset of crack growth are shown in Fig. 5, and there is no significant effect of the rate of test on the values of G_{Ic}^m, G_{IIc}^m and $G_{I/IIc}$.

4.2. End-loaded split (ELS mode II) specimens

4.2.1. Load versus time traces

The load versus time traces for the PEEK/unidirectional carbon-fibre composites tested at three different rates of test are shown in Fig. 6. Similar traces were recorded for the epoxy-composite material. Several interesting points emerge from these data.

Firstly, at the lowest rate of test, the load versus time trace (see Fig. 6a) shows that the load increases until the onset of crack propagation, when the crack initiates in an unstable manner and rapidly propagates to the end of the specimen.

Secondly, as the rate is increased there is an increasing number of oscillations on the traces which arise from dynamic effects, for example compare Fig. 6a, b and c. These oscillations obscure the unstable nature of the crack propagation, which was clearly recorded using the high-speed camera, and make it impossible to assign an unambiguous value to the load required for the crack-initiation event. As was discussed earlier, the load versus time signals were never filtered, because it is not possible to know which part of the signal represents the true behaviour of the specimen and which part reflects the purely dynamic effects.

Thirdly, these dynamic effects are likely to arise from several causes. The initial peak in the load versus time trace is very likely to be greatly influenced by inertial effects. On the other hand, the following multiple oscillations are likely to be caused by stress waves propagating in the specimen. Another possible cause of the multiple oscillations is that the shear waves, having a frequency of about 30–50 kHz, are of the appropriate frequency to create resonant effects in the piezo-electric load cell. The load cell has a natural frequency of about 70 kHz, but this is lowered somewhat when the loading shackles are connected to the cell.

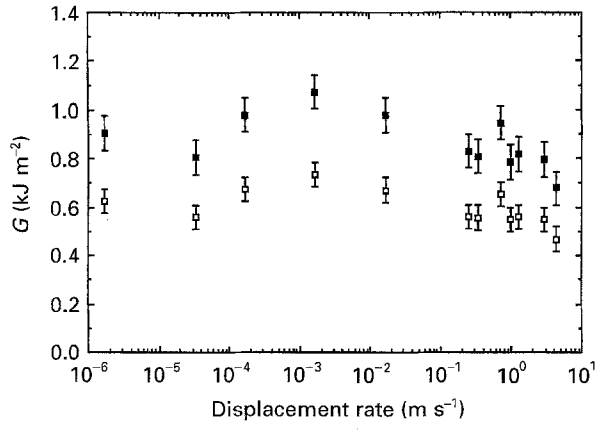

Figure 4 G_{Ic}^m and G_{IIc}^m versus specimen displacement rate for the PEEK/carbon-fibre composite. (■) G_{Ic}^m; (□) G_{IIc}^m.

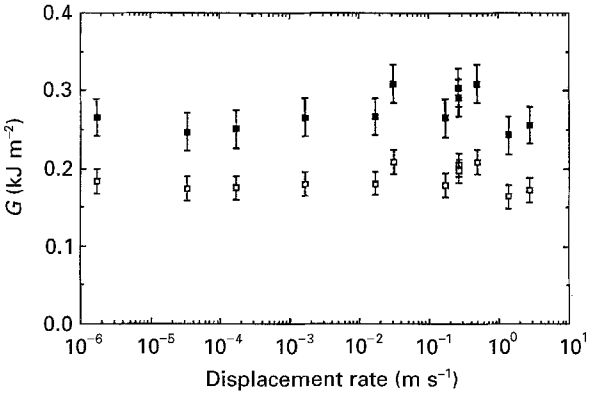

Figure 5 G_{Ic}^m and G_{IIc}^m versus specimen displacement rate for the epoxy/carbon-fibre composite. (■) G_{Ic}^m; (□) G_{IIc}^m.

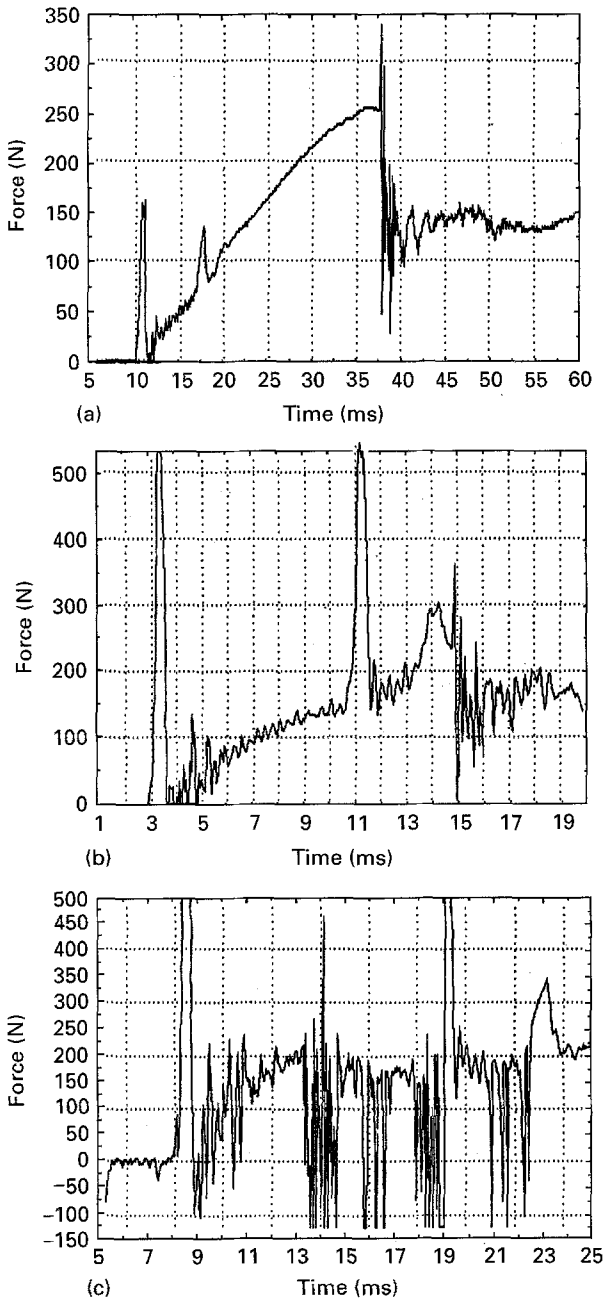

Figure 6 Typical load versus time traces for PEEK/carbon-fibre composite tests conducted at a ram-displacement rate of (a) 1 m s^{-1} (b) 2 m s^{-1} (c) 3 m s^{-1}.

Finally, as mentioned above, the dynamic effects lead to the problem that, whilst the load versus time traces obtained at the lowest test rates can be readily interpreted and analysed to yield values of the interlaminar fracture energies, the traces from the higher rates of test cannot be readily interpreted. It is for these reasons that Equations 1, 2 and 6 were derived, which enables the values of the fracture energy to be obtained without requiring a knowledge of the load applied to the specimen. However, it should be noted, as was discussed in Part II [7], that these Equations are derived from a "steady-state" analysis and they do not take into account the transient effects. Such effects, and subsequent modifications which are needed to these static analyses, are discussed in the Appendix. In the present experiments, the dynamic effects are shown not to significantly affect the values of $G_{I/IIc}$ and G_{IIc} determined using Equations 2 and 6.

4.2.2. Values of G_{IIc}

For the end-loaded split (ELS) tests, the values of G_{IIc} were obtained using Equation 6. For these tests, of course, the loading is pure mode II.

In the case of the PEEK/unidirectional carbon-fibre composite, the crack propagation was always unstable at rates in excess of 1.67×10^{-5} m s^{-1}, with the crack propagating directly to $a = L$. Thus, again, only crack initiation values could be obtained over most of the test rates employed. The effect of rate on the initiation values of G_{IIc} are shown in Fig. 7 and, as may be seen, there is no major effect of rate upon the values of G_{IIc}, although a modest reduction in the value of G_{IIc} is apparent at the higher rates. This observation is in good agreement with the results reported by Maikuma *et al.* [9] who recorded a decrease of about 28% in the value of G_{IIc} upon going from a slow-speed test to an impact test. However, the previous work of Smiley and Pipes [10] had reported far larger decreases, of the order of 80%.

For the epoxy/unidirectional carbon-fibre composite, the values of G_{IIc} as a function of the specimen-displacement rate are shown in Fig. 8. For this composite, crack propagation was stable up to a somewhat higher rate of test, of 1×10^{-3} m s^{-1}, but at higher test rates the crack propagation was again unstable. For this material the test rate clearly has no significant effect on the value of G_{IIc}.

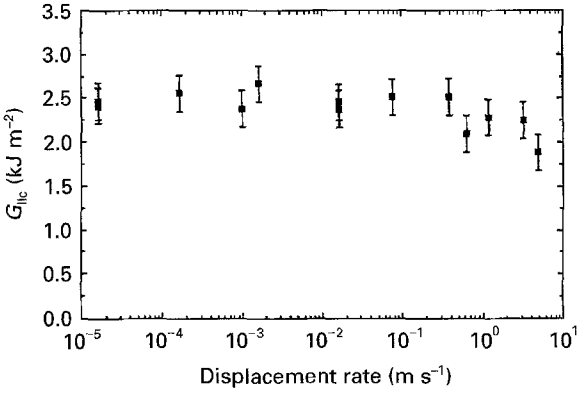

Figure 7 G_{IIc} versus specimen displacement rate for the PEEK/carbon-fibre composite.

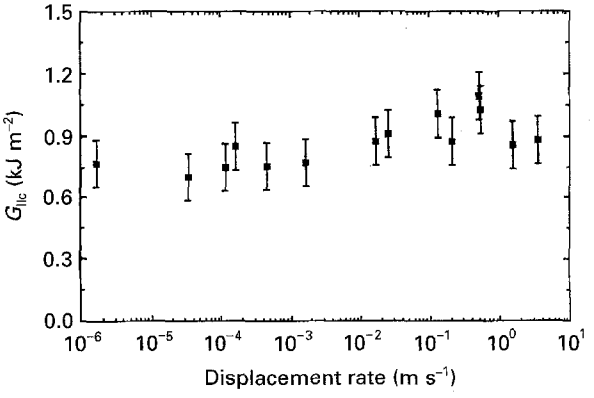

Figure 8 G_{IIc} versus specimen displacement rate for the epoxy/carbon-fibre composite.

4.3. Locus of failure curves

The failure loci curves, i.e. the curves showing the values of G_{Ic}^{m} versus G_{IIc}^{m}, for a relatively slow and a fast rate of test are shown in Figs 9 and 10 for the PEEK/unidirectional carbon-fibre and the epoxy/unidirectional carbon-fibre composites, respectively. The data from the DCB, FRMM and ELS tests are represented for each material at the two different rates.

Fig. 9 shows that for the PEEK/unidirectional carbon-fibre composite there has been a relatively consistent decrease in the interlaminar fracture energies upon going from the slowest test rate, of about $10^{-4}\,m\,s^{-1}$, to a high rate of test of $3\,m\,s^{-1}$. The decreases in the values of the interlaminar fracture energies are of the order of 20%.

However, the values of G_{Ic}^{m} versus G_{IIc}^{m} for the epoxy/unidirectional carbon-fibre composite remain quite insensitive to the test rate which was employed. Thus, the form of the failure locus was not significantly dependent upon the test rate, as can be seen from Fig. 10.

Now, in a recent paper, Charalambides *et al.* [11] have proposed a general criterion for mixed-mode failure. This criterion assumes that, at failure, a crack loaded with G_I and G_{II} will have a locally induced mode I component equal to the failure value, termed G_0, such that

$$G_0 = G_c[\cos^2(\psi - \psi_0) + \sin^2\omega \sin^2(\psi - \psi_0)] \quad (7)$$

where G_c is the measured fracture energy, ψ is the phase angle of the applied loads (with $\tan^2\psi = G_{II}/G_I$), ψ_0 is the phase angle which was suggested to arise from the elastic mismatch across a bimaterial interface (e.g. a fibre/matrix interface) and where ω was regarded as the slope of the fracture surface roughness. This equation may be fitted to the failure loci which are shown in Figs 9 and 10. As may be seen, Equation 7 provides a good description of the failure loci, and Table I gives the values of the various parameters, G_0, ω and ψ_0, needed to fit Equation 7 to the failure loci for the two composite materials, when tested at either the slow or fast rate.

Clearly, from Figs 9 and 10, Equation 7 does provide a good theoretical description of the experimental results, as would be expected with three parameters (i.e. G_0, ω and ψ_0) available for fitting the general criterion stated in Equation 7. However, it should be noted, that on inspection of the values of the parameters ω and ψ_0 in Table I, it is difficult to interpret these values in terms of the observed fracture surface features. For example, the value of ω is about 50° for the PEEK and about 40° for the epoxy composites, respectively. The parameter ω was proposed to be related to the surface roughness of the fracture surface, but it is difficult to relate any specific surface topographical features to the values of ω for the two different composites. Further, there are no obvious reasons for the different values of ψ_0; the parameter ψ_0 was suggested to be related to the elastic mismatch across the fibre/matrix interface. However, it is noteworthy that a value of $\psi_0 = 0$ would also have given a good fit of the general criterion to the experimental values in all cases.

Finally, comparing the values of G_0, ω and ψ_0 from the slow rate tests to previously reported [5, 11] values, then for the epoxy/composite there is found to be very good agreement for all the parameters. For the PEEK/composite the values of G_0 and ω are in good agreement but there is a difference in the values of ψ_0; the present value of 3° being rather lower than the previously reported values of 35°–44°. This is due to a slightly different "best-fit" shape of the failure loci for the previous tests, compared to the current tests. However, the difference is within the experimental variabil-

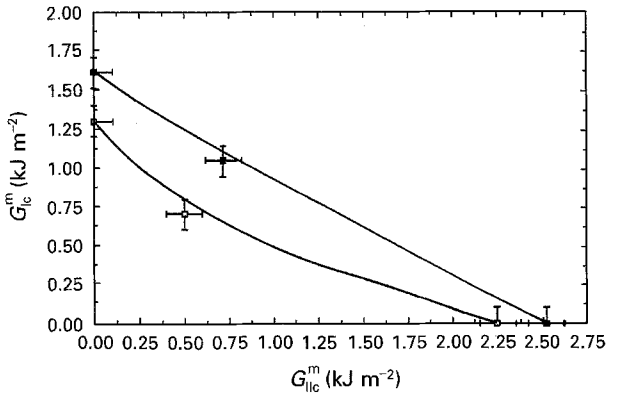

Figure 9 Values of the interlaminar fracture energies for crack initiation for the PEEK/carbon-fibre composite. Results are shown for the different modes and for two different rates of specimen displacement. The solid lines are theoretically derived from Equation 7 and the points are experimental results. (■) $2 \times 10^{-4}\,m\,s^{-1}$; (□) $3\,m\,s^{-1}$.

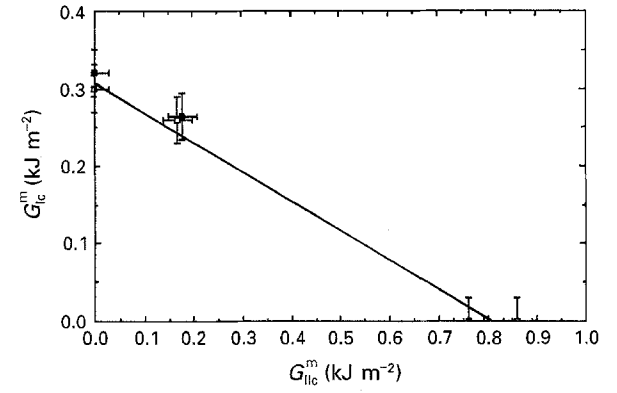

Figure 10 Values of the interlaminar fracture energies for crack initiation for the epoxy/carbon-fibre composite. Results are shown for the different modes and for two different rates of specimen displacement. (——) Theoretically derived from Equation 7; points are experimental results. (■) $2 \times 10^{-4}\,m\,s^{-1}$; (□) $3\,m\,s^{-1}$.

TABLE I Fracture criterion parameters for the composites from using Equation 7 for the "slow" and "fast" rate tests

Composite	G_0 (kJ m^{-2})	ω (deg)	ψ_0 (deg)
PEEK/composite			
slow	1.60	53	3
fast	1.30	48	10
Epoxy/composite			
slow	0.32	38	5
fast	0.32	38	5

ity seen from batch to batch testing of these materials [4, 5, 11, 12]. Thus, the conclusion to be drawn is that the value of ψ_0 is rather sensitive to the detailed shape of the failure loci curve, but the differences seen are within expected variations in the batch to batch properties of the composite. Whether such variations do basically arise from different degrees of fibre/matrix interfacial properties has yet to be established.

5. Conclusion

The present studies have discussed in detail the experimental results from studies designed to measure the mixed-mode I/II and mode II failure of fibre composites under a wide range of rates of test, up to rates of about $5\,m\,s^{-1}$.

Firstly, it has been shown that great care must be taken in the experimental aspects when undertaking the tests at high rates. For example, dynamic effects have been identified in the present studies and techniques for overcoming these problems have been reported. It is considered that, because some of the previous workers have not taken these effects into account, such effects may explain the conflicting results to be found in the literature. Of major importance in this respect is the derivation and use of expressions, for example Equations 1, 2 and 6, which do not rely upon values of the measured loads in order to deduce values of the interlaminar fracture energies, because the dynamic effects typically cause the measured loads to be unreliable and inaccurate.

Secondly, in the present experiments, the static analyses used to determine the values of $G_{I/IIc}$ and G_{IIc}, i.e. Equations 2 and 6, respectively, have been shown not to need correcting for dynamic, kinetic energy, effects. The expressions for such dynamic corrections, and those for assessing the stability of the crack growth arising from the specimen geometry, are included for completeness in the Appendix.

Thirdly, analysis of the manner in which the crack propagates has shown that, as the rate of test increases, there is an increasing tendency for unstable, "slip–stick", crack growth to be observed, although the arrest (i.e. "stick") point could not be ascertained in the present mixed-mode I/II and mode II tests, because crack growth was so unstable that the crack initiated and then grew until it reached the end of the test specimen. Comparing the results from the mode I (DCB) tests [6] to the present mixed-mode I/II (FRMM) and mode II (ELS) tests, then for the PEEK composite the type of crack growth was similar in the different test specimens. However, for the epoxy/composite, the crack growth showed a far greater tendency to be stable in nature in the mode I (DCB) tests. Thus, the type of test specimen and the type of composite material used, both influence whether stable or unstable crack propagation is observed.

Fourthly, the experimental data from the DCB, FRMM and ELS tests have allowed us to plot the failure loci curves, i.e. the curves showing the values of G_{Ic}^{m} versus G_{IIc}^{m}, for a representative "slow" and "fast" rate of test. For the PEEK/unidirectional carbon-fibre composite there is a relatively consistent decrease in the interlaminar fracture energies upon going from the slowest test rate, of about $10^{-4}\,m\,s^{-1}$, to a high rate of test of $3\,m\,s^{-1}$. The decreases in the values of the interlaminar fracture energies are of the order of 20%. However, the failure loci for the epoxy/unidirectional carbon-fibre composite remain quite insensitive to the test rate which was employed. The locus of failure curves have been described by a general mixed-mode fracture criterion. The general mixed-mode criterion assumes that at failure a crack loaded with G_I and G_{II} will have a locally induced mode I component equal to a constant value, termed G_0. Under any given mixed-mode loading condition, failure is assumed to occur when the locally induced mode I component which is acting attains the value of G_0.

Acknowledgements

The authors thank the Engineering Physical Sciences Research Council for financial support and the Polymer Engineering Group, ICI plc and Ciba Composites for general support.

Appendix. Analysis of high-speed ELS tests and FRMM tests: the kinetic energy term for dynamic *G* calculations and the stability of crack growth

A1. Mode II ELS test

A1.1. The displacement profile

Using the terminology given in Fig. A1 for a centrally cracked beam of height, $2h$, the kinetic energy in the specimen can be obtained via beam theory [13]. For the cracked arm, the second moment of area is

$$I = I_0 = 2\left(\frac{Bh^3}{12}\right) \tag{A1}$$

For the uncracked beam

$$I = \frac{B(2h)^3}{12} = 4I_0 \tag{A2}$$

Let $\xi = x/L$ and $\eta = a/L$ so that the displacement profile, u, of the beam specimen can be expressed as:

for $0 < \xi < \eta$

$$u = \frac{u_0}{2(1 + 3\eta^3)}[4\xi^3 - 3(1 + 3\eta^2)\xi + 2(1 + 3\eta^3)] \tag{A3}$$

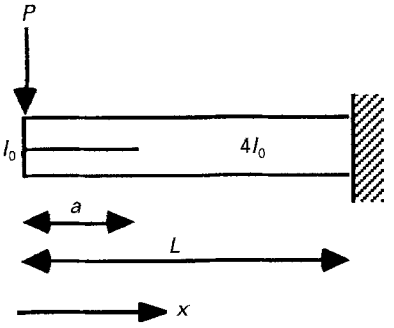

Figure A1 The terminology used for a centrally cracked beam of height $2h$.

for $\eta < \xi < 1$

$$u = \frac{u_0}{2(1+3\eta^3)}[\xi^3 - 3\xi + 2] \quad \text{(A4)}$$

where u_0 is the end displacement, and

$$u_0 = \frac{PL^3}{12E_{11}I_0}(1+3\eta^3) \quad \text{(A5)}$$

The kinetic energy, U_k in the specimen is given by

$$U_k = Bh\rho L\left(\int_0^\eta \dot{u}^2\,d\xi + \int_\eta^1 \dot{u}^2\,d\xi\right) \quad \text{(A6)}$$

where ρ is the density and $\dot{u}$ is the velocity distribution of the displacement of the beam specimen.

From Equations A3 and A4, we can obtain the velocity distribution:

for $0 < \xi < \eta$

$$\dot{u} = V\left[1 + \frac{2\xi^3 - \frac{3}{2}(1+3\eta^2)\xi}{1+3\eta^3}\right] + \frac{Vt\dot{a}}{L}\left[\frac{-18\eta\xi^3 - 9\eta\xi(1-\frac{1}{2}\eta - \frac{3}{2}\eta^3)}{(1+3\eta^3)^2}\right] \quad \text{(A7)}$$

for $\eta < \xi < 1$

$$\dot{u} = V\left[\frac{1 - \frac{3}{2}\xi + \frac{1}{2}\xi^3}{1+3\eta^3}\right] + \frac{Vt\dot{a}}{L}\left[\frac{-9\eta^2(1 - \frac{3}{2}\xi + \frac{1}{2}\xi^3)}{(1+3\eta^3)^2}\right] \quad \text{(A8)}$$

where V is the rate of test and t is the time.

In the high-speed mode II ELS tests, crack growth is unstable, and only initiation values are obtained. At initiation, the crack is stationary, so $\dot{a} = 0$. Hence we have:

for $0 < \xi < \eta$

$$\dot{u} = V\left[1 + \frac{2\xi^3 - \frac{3}{2}(1+3\eta^2)\xi}{1+3\eta^3}\right] \quad \text{(A9)}$$

for $\eta < \xi < 1$

$$\dot{u} = V\left[\frac{1 - \frac{3}{2}\xi + \frac{1}{2}\xi^3}{1+3\eta^3}\right] \quad \text{(A10)}$$

Using Equations A6, A9 and A10 we can obtain the kinetic energy term associated with the dynamic G

$$\frac{dU_k}{Bda} = E_{11}h\left(\frac{V}{c}\right)^2\left[\frac{\eta^2}{(1+3\eta^3)^3}\left(-\frac{297}{70} + 9\eta - \frac{9}{2}\eta^2 + \frac{9}{5}\eta^4 + \frac{27}{10}\eta^5 + \frac{459}{70}\eta^7\right)\right] \quad \text{(A11)}$$

where c is the wave speed of the material, and $c = (E_{11}/\rho)^{1/2}$, where E_{11} is the axial modulus of the composite.

A1.2. Dynamic G_{II} values

Now, if the dynamic value of the interlaminar fracture energy is given by G_D and the static value is given by G_{ST}, then

$$G_D = G_{ST} - \frac{dU_k}{Bda} \quad \text{(A12)}$$

From Equation A12 we may obtain for mode II loading

$$G_{ST} = \frac{9E_{11}h^3u_0^2}{L^4}\left[\frac{\eta^2}{(1+3\eta^3)^2}\right] \quad \text{(A13)}$$

and so the dynamic value under mode II loading is given by

$$G_D = \frac{9E_{11}h^3u_0^2}{L^4}\left[\frac{\eta^2}{(1+3\eta^3)^2}\right] - E_{11}h\left(\frac{V}{c}\right)^2\left[\frac{\eta^2}{(1+3\eta^3)^3}\left(-\frac{297}{70} + 9\eta - \frac{9}{2}\eta^2 + \frac{9}{5}\eta^4 + \frac{27}{10}\eta^5 + \frac{459}{70}\eta^7\right)\right] \quad \text{(A14)}$$

For a typical high-rate mode II ELS test on the epoxy composite specimen, $V = 5\,m\,s^{-1}$ and $\eta = 0.6$, the kinetic energy term is about $5\,J\,m^{-2}$, which is less than 1% of the static interlaminar fracture energy of the epoxy composite ($G_{IIc} \approx 800\,J\,m^{-2}$).

A2. The mixed-mode I/II FRMM test

A2.1. The displacement profile

In this case, the specimen has one arm loaded and the other is free to move. Using the same notation as above, we can obtain the displacement profile.

For $0 < \xi < \eta$

$$u = \frac{u_0}{2(1+7\eta^3)}[8\xi^3 - 3(1+7\eta^2)\xi + 2(1+7\eta^3)]$$

for the loaded arm (A15)

$$u = \frac{u_0}{2(1+7\eta^3)}[3(\eta^2-1)\xi + 2(1-\eta^3)]$$

for the unloaded arm (A16)

For $\eta < \xi < 1$

$$u = \frac{u_0}{2(1+7\eta^3)}[\xi^3 - 3\xi + 2] \quad \text{(A17a)}$$

where

$$u_0 = \frac{PL^3}{12E_{11}I_0}(1+7\eta^3) \quad \text{(A17b)}$$

is the end displacement at the loading point.

At crack initiation ($\dot{a} = 0$) and under a constant loading rate, V, the velocity distribution can be obtained.

For $0 < \xi < \eta$

$$\dot{u} = \frac{V}{2(1+7\eta^3)}[8\xi^3 - 3(1+7\eta^2)\xi + 2(1+7\eta^3)]$$

for the loaded arm (A18)

$$\dot{u} = \frac{V}{2(1+7\eta^3)}[3(\eta^2-1)\xi + 2(1-\eta^3)]$$

for the unloaded arm (A19)

For $\eta < \xi < 1$

$$\dot{u} = \frac{V}{2(1+7\eta^3)}(\xi^3 - 3\xi + 2) \quad \text{(A20)}$$

Now, combining Equations A6, A18–A20, we can obtain the kinetic energy term

$$\frac{dU_k}{Bda} = E_{11}h\left(\frac{V}{c}\right)^2 \frac{3\eta^2}{10(1+7\eta^3)^3}(-33 + 30\eta - 15\eta^2 + 34\eta^4 + 21\eta^5 + 139\eta^7) \quad \text{(A21)}$$

A2.2 Dynamic mixed-mode $G_{I/II}$ values

From Equations A12 and A21, and Equations 2a and b and 4, we may obtain the dynamic value under mixed-mode I/II loading

$$G_D = \frac{21E_{11}h^3u_0^2}{L^4}\left[\frac{\eta^2}{(1+7\eta^3)^2}\right] - E_{11}h\left(\frac{V}{c}\right)^2 \frac{3\eta^2}{10(1+7\eta^3)^3}(-33 + 30\eta - 15\eta^2 + 34\eta^4 + 21\eta^5 + 139\eta^7) \quad \text{(A22)}$$

Thus, for a typical high-rate, mixed-mode I/II, FRMM test on the epoxy composite specimen with $V = 5\,\mathrm{m\,s^{-1}}$ and $\eta = 0.6$, the kinetic energy term is about $12\,\mathrm{J\,m^{-2}}$, which is less than 3% of the static interlaminar fracture energy of the epoxy composite ($G_{I/IIc} \approx 500\,\mathrm{J\,m^{-2}}$).

A3. Stability of crack growth

The *geometrical* stability condition assuming a material has a constant interlaminar fracture energy, is given by

$$\frac{dG}{da} < 0 \quad \text{(A23)}$$

For the mode II ELS and the mixed-mode I/II FRMM tests, the stability condition can be written as

$$\frac{dG}{d\eta} < 0 \quad \text{(A24)}$$

Thus, for the mode II ELS tests, we have

$$2 - 12\eta^3 - A\left[\left(-\frac{297}{35} + 27\eta - 18\eta^2 + \frac{54}{5}\eta^4 + \frac{189}{10}\eta^5 + \frac{459\times 9}{70}\eta^7\right) - \frac{27\eta^3}{1+3\eta^3}\left(-\frac{297}{70} + 9\eta - \frac{9}{2}\eta^2 + \frac{9}{5}\eta^4 + \frac{27}{10}\eta^5 + \frac{459}{70}\eta^7\right)\right] < 0 \quad \text{(A25a)}$$

where

$$A = \frac{L^4}{9h^2u_0^2}\left(\frac{V}{c}\right)^2 \quad \text{(A25b)}$$

Similarly, for the mixed-mode I/II FRMM tests we have

$$2\eta(1-14\eta^3) - B\left[-\frac{9\eta}{10(1+7\eta^3)}(22 - 30\eta + 20\eta^2 - 539\eta^3 + 352\eta^4 - 224\eta^5 - 179\eta^7 + 98\eta^8)\right] < 0 \quad \text{(A26a)}$$

where

$$B = \frac{L^4}{42h^2u_0^2}\left(\frac{V}{c}\right)^2 \quad \text{(A26b)}$$

In the static case, then $A = 0$ and the stability conditions are given by $\eta \geqslant 0.55$ for mode II ELS tests, and $\eta \geqslant 0.41$ for mixed-mode FRMM tests.

For typical composite tests at $V = 5\,\mathrm{m\,s^{-1}}$, $A \approx 0.01$–0.06 and $B \approx 0.002$–0.013 and we can plot the function of the left-hand side of the inequality versus a/L. Figs A2 and A3 therefore show the stability for mode II ELS tests ($A = 0.06$) and mixed-mode I/II FRMM tests ($B = 0.013$). It can be seen that by

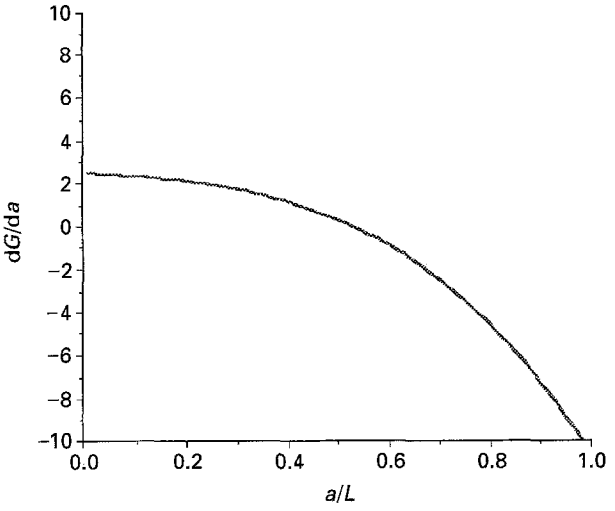

Figure A2 Stability condition for the mode II ELS tests.

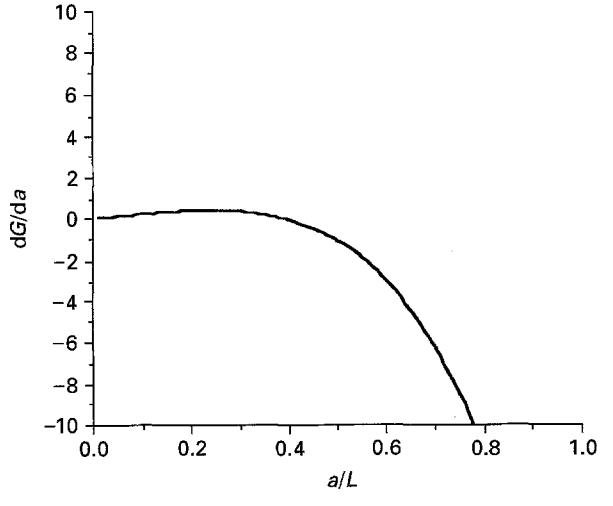

Figure A3 Stability condition for the mixed-mode I/II FRMM tests.

taking $a/L > 0.6$, the geometrical stability condition is satisfied for both the mode II ELS test and the mixed-mode I/II FRMM test.

References

1. J. M. WHITNEY, C. E. BROWNING and W. HOOGSTEDEN, *J. Reinf. Plast. Compos.* **1** (1982) 297.
2. P. E. KEARY, L. B. ILCEWICZ, C. SHAAR and J. TROSTLE, *J. Compos. Mater.* **19** (1985) 154.
3. S. HASHEMI, A. J. KINLOCH and J. G. WILLIAMS, *Proc. R. Soc.* **A427** (1990) 173.
4. *Idem, J. Compos. Mater.* **24** (1990) 918.
5. A. J. KINLOCH, Y. WANG, J. G. WILLIAMS and P. YAYLA, *Compos. Sci. Technol.* **47** (1993) 225.
6. B. R. K. BLACKMAN, J. P. DEAR, A. J. KINLOCH, H. M. MacGILLIVRAY, Y. WANG, J. G. WILLIAMS and P. YAYLA, *J. Mater. Sci.* **30** (1995) 5885.
7. B. R. K. BLACKMAN, A. J. KINLOCH, Y. WANG and J. G. WILLIAMS, *ibid.* **31** (1996) 4451.
8. Y. WANG and J. G. WILLIAMS, *Compos. Sci. Technol.* **43** (1992) 251.
9. H. MAIKUMA, J. W. GILLESPIE and D. J. WILKINS, *J. Compos. Mater.* **24** (1990) 124.
10. A. J. SMILEY and R. B. PIPES, *Compos. Sci. Technol.* **29** (1987) 1.
11. M. CHARALAMBIDES, A. J. KINLOCH, Y. WANG and J. G. WILLIAMS, *Int. J. Fract.* **54** (1992) 269.
12. I. N. DYSON, A. J. KINLOCH and A. OKADA, *Composites* **25** (1994) 189.
13. J. G. WILLIAMS, *J. Strain Anal.* **28** (1993) 247.

Received 19 January
and accepted 18 March 1996